Chemoradiation Therapy

International Edition: DOI: 10.1002/anie.201902612
German Edition: DOI: 10.1002/ange.201902612

A Catalase-Like Metal-Organic Framework Nanohybrid for O_2-Evolving Synergistic Chemoradiotherapy

Zhimei He[+], Xiaolin Huang[+], Chen Wang[+], Xiangli Li, Yijing Liu, Zijian Zhou, Sheng Wang, Fuwu Zhang, Zhantong Wang, Orit Jacobson, Jun-Jie Zhu, Guocan Yu,* Yunlu Dai,* and Xiaoyuan Chen**

Abstract: *Tumor hypoxia, the "Achilles' heel" of current cancer therapies, is indispensable to drug resistance and poor therapeutic outcomes especially for radiotherapy. Here we propose an in situ catalytic oxygenation strategy in tumor using porphyrinic metal-organic framework (MOF)-gold nanoparticles (AuNPs) nanohybrid as a therapeutic platform to achieve O_2-evolving chemoradiotherapy. The AuNPs decorated on the surface of MOF effectively stabilize the nanocomposite and serve as radiosensitizers, whereas the MOF scaffold acts as a container to encapsulate chemotherapeutic drug doxorubicin. In vitro and in vivo studies verify that the catalase-like nanohybrid significantly enhances the radiotherapy effect, alleviating tumor hypoxia and achieving synergistic anticancer efficacy. This hybrid nanomaterial remarkably suppresses the tumor growth with minimized systemic toxicity, opening new horizons for the next generation of theranostic nanomedicines.*

Hypoxia, a phenotype of inadequate O_2 supply in fast-growing tumors due to the aberrant and tortuous tumor vasculature, is highly responsible for tumor migration, invasion, metastasis, and resistance to different therapies.[1] Massive evidences have shown that hypoxic cells are less sensitive to radiation damage than normoxic cells in radiotherapy.[2] On account of this, elevation of tumor O_2 is highly expected to benefit the radiotherapy. Quite different from hyperbaric oxygen therapy suffering from safety concerns and ineffective outcomes,[3] smart nanomedicines carrying O_2-generating agents (e.g., catalase, MnO_2) can produce O_2 triggered by external light and/or unique pathological stimuli,[4] providing potent strategies to reprogramm tumour hypoxia to promote O_2-enhanced radiotherapy. Alternatively, to maximize the responses in a given dose of radiation, high-Z materials are recommended to sensitize hypoxic cells to radiation, among which gold nanoparticles (AuNPs) are outstanding candidates owing to their large X-ray attenuation coefficient. The introduction of AuNPs facilitates the efficient deposition of irradiation energy within the tumor, making the best utilization of radiation.[2b,5]

In the clinic, radiotherapy is usually utilized as an adjuvant tool to combine with surgery or chemotherapy to lessen the chance of tumor recurrence.[6] So far, although continuous efforts have been invested in the combined chemoradiotherapy, their anti-tumor performances are often unsatisfactory due to tumor resistance to treatments. Therefore, it is urgently required to develop smart nanoparticles (NPs) capable of generating O_2 in situ, amplifying radiation signals and regulating drug release on command, so as to synergistically eradicate tumor. Porphyrin-based metal-organic framework (MOF) NPs are a kind of crystalline hybrid materials made up of metal ions/clusters and organic building units (porphyrins or metalloporphyrins). Owing to their high storage capacities, compositions tailorability, biodegradability and feasible modifiability or functionality,[7] porphyrinic MOF NPs have emerged as potent platforms for photodynamic therapy and delivery of theranostic agents.

Herein, we engineered a biodegradable nanocomposite featuring stimuli-responsive O_2 generation as well as controlled drug release for O_2-elevated chemoradiotherapy. The nanohybrid (MOF-Au) was constructed by in situ growth of AuNPs onto the surface of porphyrinic MOF NPs (Figure 1). The decoration of AuNPs brought about several attractive advantages: (i) serving as radiosensitizers to boost radiotherapy; (ii) facilitating efficient PEGylation to prevent the aggregation of the NPs in physiological environment; and (iii) endowing the MOF NPs with relatively high stability against phosphate to prevent premature degradation during blood circulation. Interestingly, the MOF-Au with PEGylation worked as an artificial enzyme to oxygenate tumor micro-

[*] Dr. Z. He,[+] X. Li, Prof. J.-J. Zhu
State Key Laboratory of Analytical Chemistry for Life Science
School of Chemistry and Chemical Engineering, Nanjing University
Nanjing 210023 (P. R. China)
E-mail: jjzhu@nju.edu.cn

Dr. X. Huang[+]
State Key Laboratory of Food Science and Technology
School of Food Science and Technology, Nanchang University
Nanchang 330047 (P. R. China)

Dr. C. Wang[+]
State Key Laboratory of Pharmaceutical Biotechnology
School of Life Sciences, Nanjing University
Nanjing 210093 (P. R. China)

Dr. Y. Liu, Dr. Z. Zhou, Dr. S. Wang, Dr. F. Zhang, Dr. Z. Wang, Dr. O. Jacobson, Dr. G. Yu, Prof. X. Chen
Laboratory of Molecular Imaging and Nanomedicine (LOMIN)
National Institute of Biomedical Imaging and Bioengineering (NIBIB), National Institutes of Health (NIH)
Bethesda, MD 20892 (USA)
E-mail: guocan.yu@nih.gov
shawn.chen@nih.gov

Dr. Y. Dai
Faculty of Health Sciences, University of Macau
Macau SAR 999078 (P. R. China)
E-mail: yldai@umac.mo

[+] These authors contributed equally to this work.

Supporting information and the ORCID identification number(s) for the author(s) of this article can be found under: https://doi.org/10.1002/anie.201902612.

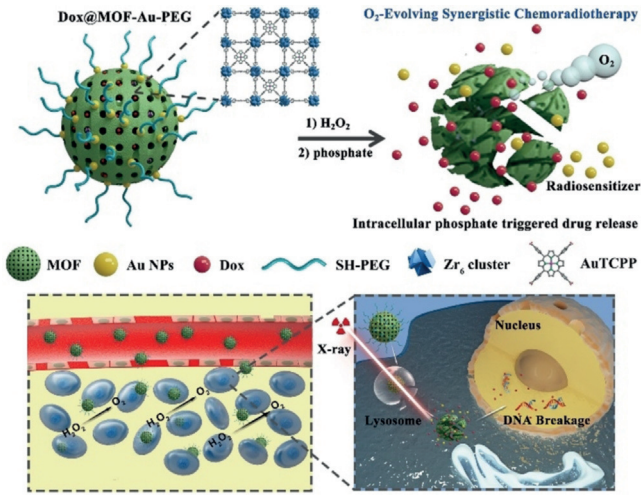

Figure 1. Schematic representation showing the main components of Dox@MOF-Au-PEG and the mechanism of O_2 self-supplying synergistic chemoradiotherapy.

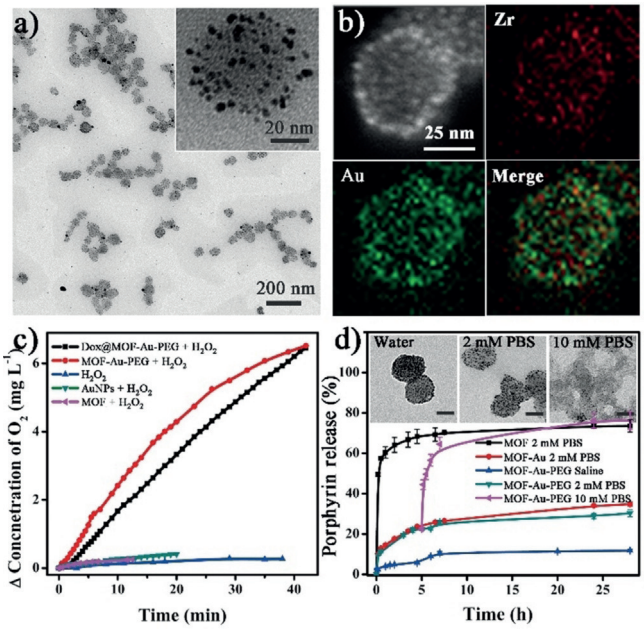

Figure 2. a) TEM images and b) EDS mapping of MOF-Au NPs. c) O_2 generation by various samples with normalized MOF weight (1 mg mL^{-1}) in the presence of H_2O_2 at a physiological concentration of 400 μM. d) Release profiles of the porphyrin ligand under different conditions. Insets: TEM images of MOF-Au-PEG after incubation with water or PBS for 24 h.

environment by catalyzing tumor metabolites H_2O_2 into O_2, which was beneficial to O_2-dependent radiotherapy. Furthermore, the MOF covered by AuNPs still remained highly porous through well regulation, allowing to load anticancer drug doxorubicin (Dox). Both in vitro and in vivo studies demonstrated that the nanomedicine exhibited superior anticancer efficacy with negligible systematic toxicity, attributing to the synergistic effect of chemoradiotherapy.

The MOF-Au hybrid was obtained through an in situ growth method by reducing $HAuCl_4$ into AuNPs on the surface of MOF.[7b,8] The successful fabrication of MOF-Au was verified by transmission electron microscopy (TEM) (Figure 2a and Figure S1 in the Supporting Information), energy dispersive spectroscopy (EDS) mapping (Figure 2b), X-ray photoelectron spectroscopy (XPS) spectra (Figure S2) and powder X-ray diffraction (PXRD) pattern (Figure S3). Gold(III) porphyrin complex (AuTCPP) was simultaneously formed during the growth of AuNPs as characterized by high-resolution XPS spectra (Figure S2) and UV/Vis spectra (Figure S4). It should be pointed out that the crystallinity and unique porous structure of MOF platform in the MOF-Au hybrid was greatly maintained during the preparation of MOF-Au, which was confirmed by PXRD pattern (Figure S3) and N_2 adsorption-desorption isotherm measurement (Figure S5), suggesting that the MOF scaffold was a perfect candidate to encapsulate therapeutic cargoes (e.g., Dox). To avoid nonspecific adsorption of Dox by AuNPs, MOF-Au NPs were PEGylated (MOF-Au-PEG) that was verified by the hydrodynamic diameter (Figure S6) and zeta potential (Figure S7) changes. Then Dox was loaded into MOF-Au-PEG driven by the π-π interaction between Dox and the porphyrin ligands. Attributing to the presence of densely packed PEG corona, the fabricated NPs (Dox@MOF-Au-PEG) were well dispersed in saline solution, PBS (2 mM) and cell culture medium (Figure S8), making them suitable for biomedical applications.

Interestingly, we uncovered that the MOF-Au-PEG nanohybrid possessed catalytic activity in decomposing H_2O_2 according to the O_2 generation profile (Figure 2c). Moreover, drug encapsulation had little effect on the catalytic property of MOF-Au-PEG NPs, as evidenced by their good performance in O_2 generation. In contrast, AuNPs or MOF alone contributed little to O_2 production under the same condition. Given the abundance of tumor metabolites H_2O_2 and the radiosensitization of both AuNPs and O_2,[4a,5,9] such catalase-like activity makes Dox@MOF-Au-PEG promising in elevating O_2 tension in tumor tissue to further boost AuNPs-sensitized radiotherapy.

The envelopment of MOF-Au-PEG NPs by AuNPs shielded them against phosphate attack to some extent. Owing to the stronger coordination interaction between phosphate ion and zirconium,[10] the MOF readily decomposed in PBS (2 mM), manifesting by the burst release of porphyrin ligands (Figure 2d) and structure collapse (Figure S9). In stark contrast, MOF-Au NPs displayed much improved phosphate tolerance with much slower release rate of porphyrin in PBS (2 mM). Several possible reasons were responsible for the stability improvement: (i) A protective shield of AuNPs was formed, masking the MOF from phosphate attack; (ii) The surface zeta potential changed from being positive to negative (Figure S10) after AuNPs growth, avoiding the electrostatic interaction between the MOF and phosphate; (iii) The AuNPs could act as the physical crosslinks to further stabilize the MOF scaffold. Additionally, the PEG shell on the surface further stabilized MOF-Au-PEG against the phosphate attack. When the concentration of PBS increased to 10 mM, rapid release of porphyrin (Figure 2d) and shedding of AuNPs (Figure S11) occurred along with the framework collapse (Figure S9).

Similarly, Dox@MOF-Au-PEG presented phosphate-sensitive drug release behavior (Figure S12). Hence, it is highly expected that the MOF-Au-PEG NPs with relatively high stability remain intact in extracellular/plasma fluid, of which the phosphate level is about 2 mM.[11] Upon internalization by cancer cells, the high concentration of phosphate in cells[10,11] may lead to disintegration of the NPs. After 24 h dispersion in cell culture medium, little change in both morphology (Figure S13a) and hydrodynamic diameter (Figure S13b) was observed, indicating the good stability of MOF-Au-PEG NPs in culture medium. The co-existence of Au and Zr insides U87MG cells confirmed that the MOF-Au-PEG NPs could be readily taken up by cells (Figure S14). As predicted, MOF-Au-PEG NPs became fragmented inside cells according to the TEM analysis (Figure S15 and Figure 3a). The degradation of MOF-Au-PEG NPs also benefited the liberation of Dox and the ligand tetrakis(4-carboxyphenyl)porphyrin (H_2TCPP), accompanied by their fluorescence recovery (Figures S16 and S17). On account of this, confocal laser scanning microscopy (CLSM) imaging was employed to confirm the intracellular drug release behavior by monitoring the restored fluorescence of the liberated Dox and H_2TCPP. The fluorescence of both Dox and H_2TCPP was clearly observed in the cells (Figures 3b and S18) showing a time-dependent internalization. Notably, intranuclear accumulation of Dox increased as the incubation time extended, which implied the efficient drug release followed by the disassembly of Dox@MOF-Au-PEG. Overall, the Dox@MOF-Au-PEG NPs featuring efficient transportation into cells and sensitive intracellular drug release provides a potent strategy in potentiating therapeutic efficacy.

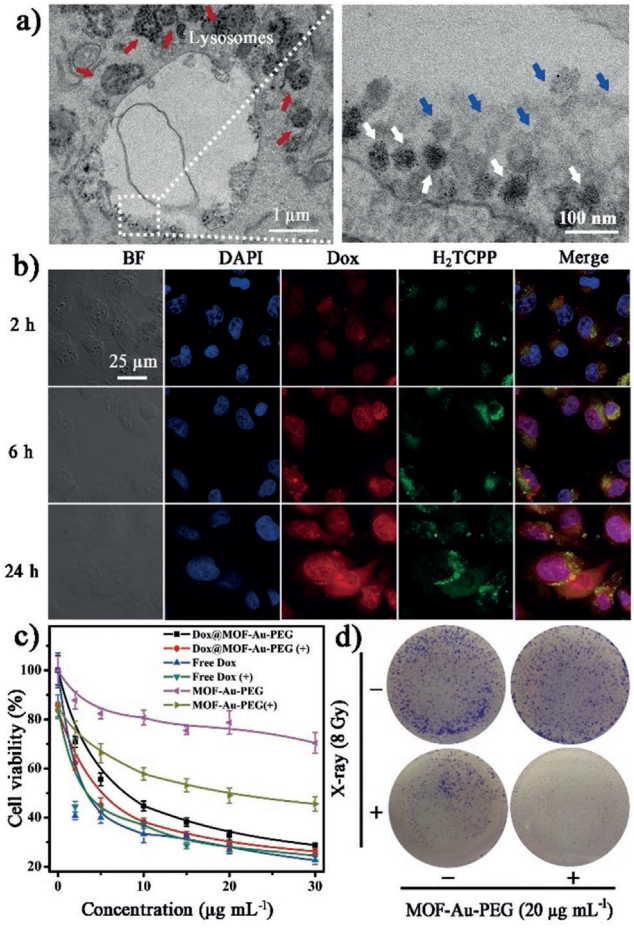

Figure 3. a) Bio-TEM images of U87MG cells after treatment with MOF-Au-PEG for 24 h. Arrows: purplish red, lysosomes; white, intact NPs with massive coating of small dark spots (AuNPs); blue, collapsed NPs manifested fewer decorations of AuNPs along with lighter contrast. b) CLSM images of U87MG cells treated with Dox@MOF-Au-PEG for different periods of time. c) Cell survival rate and d) colon formation of U87MG cells after different treatments. Opposed to (−), (+) denotes X-ray was applied in the group. The concentration shown in (c) and (d) represents the normalized concentration of MOF.

In this work, we integrated the radiosensitization effect of AuNPs with the anticancer effect of Dox for combined radiochemotherapy. 3-(4′,5′-Dimethylthiazol-2′-yl)-2,5-diphenyltetrazoliumbromide (MTT) assay was utilized to assess the synergistic anticancer efficacy against U87MG cells. The administration of single X-ray radiation (8 Gy) resulted in limited anticancer outcome, showing 15% inhibition of cell proliferation (Figure 3c). For MOF-Au-PEG, slight cell inhibition was observed likely caused by the anticancer activity of AuTCPP chelates.[12] Notably, the treatment with MOF-Au-PEG followed by X-ray radiation (denoted as + hereafter) imposed more substantial suppression on cell viability in a dose-dependent manner owing to the radiosensitization of AuNPs. Dox@MOF-Au-PEG (+) presented excellent cytotoxicity, which was comparable to that of free Dox (+) possessing brilliant anticancer ability due to its extremely efficient cellular internalization. From the MTT assay (Figures 3c and S19), negligible difference in cell survival rate between free Dox and free Dox (+) was observed, while Dox@MOF-Au-PEG (+) exhibited higher cell inhibition than that of Dox@MOF-Au-PEG, implying the radiosensitization of the nanocarrier. The combination index (CI) of Dox@MOF-Au-PEG (+) was determined to be 0.88, confirming the synergistic anticancer efficacy of chemoradiotherapy. Since short-term MTT assay is less common to study survival of irradiated cells,[13] clonogenic assay was conducted to determine the efficiency of MOF-Au-PEG radiosensitizer for accurate comparison (Figure 3d). It was found that the MOF-Au-PEG (+) showed much higher chronic cytotoxicity than those of MOF-Au-PEG and X-ray alone, thus verifying the radiotherapy-enhancing effect of the MOF-Au-PEG NPs. In DNA double-strand breaks study, Dox@MOF-Au-PEG (+) treated cells emitted the most intense γH_2AX fluorescence attributing to the severe DNA damage (Figure S20), demonstrating the superior efficacy of the radiochemotherapy.

Prior to in vivo therapy, the biodistribution of the nanomedicine was investigated on U87MG tumor-bearing female nude mice using positron emission tomography (PET) imaging. Obvious tumor signal with a high tumor-to-background contrast was observed in the mice receiving intravenous (i.v.) injection of ^{64}Cu-labeled MOF-Au-PEG (^{64}Cu-MOF-Au-PEG) (Figure 4a). Quantitative region of interest (ROI) analysis was applied to determine the corresponding time-dependent biodistribution of the nanohybrid (Figure 4b). Notably, the retention of the ^{64}Cu-MOF-Au-PEG in blood

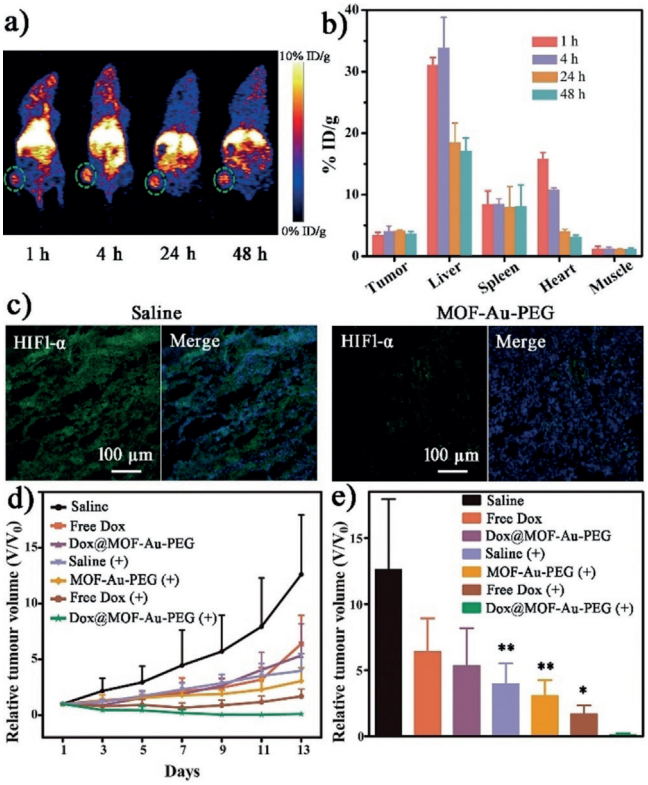

Figure 4. a) PET imaging of U87MG tumor-bearing mice at different time points p.i. of ^{64}Cu-MOF-Au-PEG. The green dashed circles represent the tumor locations. b) Quantitative ROI assay of major tissues ($n=3$). c) HIF1-α immunofluorescence analysis of the tumor slices collected at 8 h p.i of saline or MOF-Au-PEG. d) Tumor growth curves of the mice administered with different treatments ($n=5$). e) The final relative tumor volume on day 13 after various treatments. $^{*}p<0.05$ vs. Dox@MOF-Au-PEG. $^{**}p<0.01$ vs. Dox@MOF-Au-PEG.

still remained at 10.78% at 4 h post injection (p.i.) by quantifying the ^{64}Cu signal in the heart (Figures 4b and S21), demonstrating the prolonged circulation behavior of the NPs in blood. The ^{64}Cu-MOF-Au-PEG effectively accumulated in the tumor site, the amount was calculated to be 4.10% ID g^{-1} and 3.65% ID g^{-1} at 24 h and 48 h p.i., respectively, which was primarily benefited from the enhanced permeability and retention (EPR) effect. Ex vivo biodistribution quantification was carried out at 48 h p.i. using a gamma counter, in which the results matched well with those quantified from PET images (Figure S22).

Recently, tumor characteristics (e.g., hypoxia, high H_2O_2 content) have emerged as therapeutic targets to modulate tumor microenvironments and promote therapy for precise treatment.[4c,6b] On account of this, we investigated the O_2 generation capacity of MOF-Au-PEG in hypoxic cancer cells. Extraneous H_2O_2 was introduced to simulate the excessive H_2O_2 level (0.5 nmol/10^4 cells h^{-1})[4a,b] in the tumor. Significant promotion of O_2 was found in the presence of MOF-Au-PEG, in sharp contrast to the negligible generation of O_2 by H_2O_2 alone (Figure S23). Inspired by this finding, we hypothesized that the abundant tumor metabolite H_2O_2 could function as a reactant to participate in the production of O_2 in vivo. Hypoxia-inducible factor 1α (HIF1-α) immunofluorescence staining of tumor section was then employed to reflect the O_2 level. The green fluorescence indicative of hypoxia dramatically decreased in the tumor tissue from the mice treated with MOF-Au-PEG (Figure 4c). This phenomenon demonstrated the excellent performance of catalase-like MOF-Au-PEG in relieving tumor hypoxia which had been reported to be responsible for tumor resistance to radiotherapy.

Encouraged by the high tumor accumulation and subsequent in situ generation of O_2, we then evaluated the antitumor effect on U87MG tumor-bearing nude mice. The mice were intravenously injected with various formulations at a Dox-equivalent dose of 2 mg kg^{-1}, and were partly subjected to 8 Gy radiation at 24 h p.i. It was found that the tumors grew rapidly in the saline-treated group (Figure 4d and 4e). Free Dox, Dox@MOF-Au-PEG or radiation alone moderately delayed the tumor growth. Furthermore, MOF-Au-PEG (+) exerted more pronounced inhibition in tumor growth, confirming the radiosensitization effect of the nanocarrier. Excitingly, Dox@MOF-Au-PEG (+) was most effective in tumor suppression with continuous tumor shrinkage during the treatments. The corresponding tumor inhibition rate on day 13 after treatment reached 89%. Hematoxylin and eosin (H&E) staining indicated that prominently enhanced tumor necrosis was observed in the tumor slices of the mice treated with Dox@MOF-Au-PEG (+) (Figure S24). Benefiting from the modulation of tumor hypoxia, on-demand drug release and synergistic effect, efficient tumor eradication was achieved at low drug dosage to minimize systemic toxicity. As anticipated, no significant changes in body weight (Figure S25) or organ histopathology (Figure S26) were observed after the treatments. Compared to other nanocarriers, Dox@MOF-Au-PEG NPs combine many advantages, such as high storage capacities, biodegradability, self-sufficiency of O_2, on-demand drug release and combined therapies, offering valuable strategies for next-generation of nanomedicines in cancer theranostics.

In conclusion, we fabricated a PEGylated MOF-Au nanohybrid, in which AuNPs were grown in situ on the porphyrinic MOF NPs. Attributing to the surrounded compact AuNPs and a dense PEG corona, the MOF-based nanomedicine possessed a prolonged blood circulation time, which favored the tumor accumulation through EPR effect. Furthermore, the nanohybrid demonstrated catalase-like activity, on-demand drug release and enhanced radiotherapeutic efficacy, achieving synergistic radiochemotherapy. Notably, the catalase-like activity enabled the nanohybrid to elevate tumor O_2 for further enhancement of in vivo chemoradiotherapy. Such versatile nanohybrid with excellent antitumor performance will be a paradigm of O_2-elevated radiochemotherapy, offering a novel strategy in multimodal cancer therapy.

Acknowledgements

This work was supported by the National Natural Science Foundation of China (21834004, 21427807), International Cooperation Foundation from Ministry of Science and

Technology (2016YFE0130100), China Postdoctoral Science Foundation (2018M640472), the Start-up Research Grant (SRG) of University of Macau (SRG2018-00130-FHS), the Science and Technology Development Fund of Macao SAR (FDCT 0109/2018/A3 to Y.D.) and the Intramural Research Program (IRP) of National Institute of Biomedical Imaging and Bioengineering (NIBIB), National Institutes of Health (NIH).

Conflict of interest

The authors declare no conflict of interest.

Keywords: catalase-like activity · chemoradiation therapy · controlled drug release · radiosensitizer · tumour hypoxia

How to cite: *Angew. Chem. Int. Ed.* **2019**, *58*, 8752 – 8756
Angew. Chem. **2019**, *131*, 8844 – 8848

[1] a) J. Reyal, *Med. Hypotheses* **2010**, *74*, 301 – 308; b) X. Song, L. Feng, C. Liang, K. Yang, Z. Liu, *Nano Lett.* **2016**, *16*, 6145 – 6153.
[2] a) V. Hosseini, M. Mirrahimi, A. Shakeri-Zadeh, F. Koosha, B. Ghalandari, S. Maleki, A. Komeili, S. K. Kamrava, *Photodiagn. Photodyn. Ther.* **2018**, *24*, 129 – 135; b) Z. Song, Y. Chang, H. Xie, X.-F. Yu, P. K. Chu, T. Chen, *NPG Asia Mater.* **2017**, *9*, e439.
[3] M. Heyboer 3rd, D. Sharma, W. Santiago, N. McCulloch, *Adv. Wound Care* **2017**, *6*, 210 – 224.
[4] a) T. P. Szatrowski, C. F. Nathan, *Cancer Res.* **1991**, *51*, 794 – 798; b) Q. Jia, J. Ge, W. Liu, X. Zheng, S. Chen, Y. Wen, H. Zhang, P. Wang, *Adv. Mater.* **2018**, *30*, 1706090; c) Q. Chen, L. Feng, J. Liu, W. Zhu, Z. Dong, Y. Wu, Z. Liu, *Adv. Mater.* **2016**, *28*, 7129 – 7136.
[5] J. Cho, M. Wang, C. Gonzalez-Lepera, O. Mawlawi, S. H. Cho, *Med. Phys.* **2016**, *43*, 4775 – 4788.
[6] a) K. J. Son, H.-J. Yoon, J.-H. Kim, W.-D. Jang, Y. Lee, W.-G. Koh, *Angew. Chem. Int. Ed.* **2011**, *50*, 11968 – 11971; *Angew. Chem.* **2011**, *123*, 12174 – 12177; b) W. Fan, B. Yung, P. Huang, X. Chen, *Chem. Rev.* **2017**, *117*, 13566 – 13638.
[7] a) M. Lismont, L. Dreesen, S. Wuttke, *Adv. Funct. Mater.* **2017**, *27*, 1606314; b) J. Park, Q. Jiang, D. Feng, L. Mao, H.-C. Zhou, *J. Am. Chem. Soc.* **2016**, *138*, 3518 – 3525; c) R. Freund, U. Lächelt, T. Gruber, B. Rühle, S. Wuttke, *ACS Nano* **2018**, *12*, 2094 – 2105.
[8] Y. Huang, M. Zhao, S. Han, Z. Lai, J. Yang, C. Tan, Q. Ma, Q. Lu, J. Chen, X. Zhang, Z. Zhang, B. Li, B. Chen, Y. Zong, H. Zhang, *Adv. Mater.* **2017**, *29*, 1700102.
[9] G. Song, C. Liang, X. Yi, Q. Zhao, L. Cheng, K. Yang, Z. Liu, *Adv. Mater.* **2016**, *28*, 2716 – 2723.
[10] C. He, K. Lu, D. Liu, W. Lin, *J. Am. Chem. Soc.* **2014**, *136*, 5181 – 5184.
[11] L. L. Hill, *Pediatr. Clin. North Am.* **1990**, *37*, 241 – 256.
[12] a) S. Tu, R. W.-Y. Sun, M. C. M. Lin, J. T. Cui, B. Zou, Q. Gu, H.-F. Kung, C.-M. Che, B. C. Y. Wong, *Cancer* **2009**, *115*, 4459 – 4469; b) K. Laws, K. Suntharalingam, *ChemBioChem* **2018**, *19*, 2246 – 2253.
[13] K. Buch, T. Peters, T. Nawroth, M. Sänger, H. Schmidberger, P. Langguth, *Radiat. Oncol.* **2012**, *7*, 1.

Manuscript received: February 28, 2019
Revised manuscript received: April 11, 2019
Accepted manuscript online: May 2, 2019
Version of record online: May 16, 2019

